JOURNAL OF MATERIALS SCIENCE 20 (1985) 4561–4582

The nitriding behaviour of iron–chromium–carbon alloys

P. C. VAN WIGGEN, H. C. F. ROZENDAAL, E. J. MITTEMEIJER
Laboratory of Metallurgy, Delft University of Technology, Rotterdamseweg 137, 2628 AL Delft, The Netherlands

The nitriding behaviour of an FeCrC (3.16 wt% Cr, 0.20 wt% C) alloy, as a model system for En40B (a classical gas-nitriding steel), was investigated. By comparing the response of a hardened structure, a quenched and tempered structure and an annealed structure, the effect on nitriding of different initial chromium and carbon disbributions over the phases present could be studied. The structure after nitriding was described employing metallographic methods (optical and scanning electron microscopy; hardness measurements), electron microprobe analysis (concentration–depth profiles) and X-ray diffractometry (residual macrostress determination; phase identification). Further the weight and thickness increases of the specimens during nitriding were determined. During initial stages of nitriding, excess-nitrogen uptake and the development of grain-boundary carbides and a compressive residual surface macrostress took place. At later stages discontinuous precipitation, void formation, decarburization and relaxation of the compressive residual macrostress occurred. The observations lead to a model description for the nitriding of an FeCrC alloy.

1. Introduction

Nitriding of workpieces of steel can lead to significant improvement of the fatigue, anti-corrosion and tribological properties. This well-known thermochemical surface treatment can, in practice, be performed in gaseous and plasma atmospheres, in salt baths and in powders [1].

The nitrided case, in general, can be subdivided into (i) a compound layer (thickness of the order 10 μm) adjacent to the surface, and (ii) a diffusion zone (thickness of the order 0.1 mm) beneath the compound layer. The compound layer is predominantly composed of iron(carbo)nitrides. For a recent microstructural description of compound layers on iron and steels, see [2]. Beneficial anti-corrosion and tribological properties can be ascribed to certain compound layers. In this connection special variants of the nitriding process have been developed [3–6].

The diffusion zone of an alloyed steel usually contains a fine dispersion of alloying-element nitrides. The enhancement of the fatigue resistance is ascribed to macro- and microstresses provoked by these nitrides in the diffusion zone [7].

In spite of the commercial application of nitriding over 60 years, there is a general lack of knowledge relating the nitrided microstructure to the properties [2, 8]. Chromium is frequently applied as an alloying element because of its affinity to nitrogen. Recently our group performed research on the nitriding of binary FeCr alloys [9, 10], which resulted in a model for the corresponding nitriding behaviour, describing the occurrence of excess-nitrogen, discontinuous precipitation and residual macrostress development [10]. As a next step, this paper describes the nitriding behaviour of a ternary FeCrC (3.16 wt % Cr, 0.20 wt % C) alloy. This alloy can be considered as a model system for the classical gas-nitriding steel En40B (also indicated as

0022–2461/85 $03.00 + .12

24CrMo13, containing 0.20 to 0.28 wt % C and 3.00 to 3.50 wt % Cr as major alloying element). In the present work the effect on nitriding of different chromium and carbon distributions over the matrix and the carbides was studied by employing various initial heat treatments. Further, the nitriding conditions were chosen such that no compound layer at the surface of the specimen occurred. Thus the response to nitriding of a chromium-alloyed steel matrix was investigated.

2. Experimental procedures

2.1. Specimen preparation

Rectangular specimens (3 cm × 2 cm, about 110, 265, 440 and 555 μm thick; metallography, thickness and weight measurements) as well as disc-shaped specimens (diameter 20 mm, 3.5 mm thick; X-ray diffractometry) were prepared from an FeCrC alloy (3.16 wt % Cr, 0.20 wt % C, balance Fe) either in the *hardened* condition (austenitized, 45 min, 1273 K; oil quenched, 323 K), or in the *quenched and tempered* condition (austenitized, 45 min, 1273 K; oil quenched, 323 K; tempered, 60 min, 903 K; air cooled) or in the *annealed* condition (annealed, 2 h, 1073 K; 65 h, 998 K; furnace cooled). Before nitriding the specimens were mechanically polished (final stage 1 μm diamond), ultrasonically cleaned in alcohol, degreased in trichloroethane and etched in a 2% nital solution.

2.2. Nitriding procedure

Nitriding was performed in a vertical tube furnace (tube and suspension of specimen made of quartz) in a 10 vol % ammonia (Matheson; 99.96 vol %) and 90 vol % hydrogen (Hoek Loos; 99.995 vol %) gas mixture at 803 K (temperature control within 2 K). Both gases were purified by leading them through BTS-catalyst and soda lime subsequently before entering the mixing bottle. The flow rate in the furnace was about 0.8 cm sec^{-1}. Under these conditions no compound (iron nitride) layer formation occurred at the surface.

2.3. Weight measurements

Weight increase as a function of nitriding time was determined by using a Mettler balance type M5 (accuracy about 2 μg).

2.4. Thickness measurements

Thickness increase as a function of nitriding time was determined by using an electronic micrometer (Quality type SN; accuracy about 1 μm).

2.5. Metallography

Optical microscopy was performed with a Neophot-2 microscope (Carl Zeiss, Jena). In order to avoid curvature of the cross-sections close to the edges owing to mechanical polishing, segments of the specimens were provided with a nickel layer electrolytically deposited from a Watt's bath [11]. After polishing the specimens were either nital etched or etched according to Murakami. By nital etching (0.5% of nitric acid in ethanol) grain and phase boundaries are preferentially attacked. Recently it was demonstrated that Murakami etching (10 g $K_3Fe(CN)_6$ in a 10% solution of KOH in distilled water) provides a sensitive discrimination between pure nitrides and carbon-containing nitrides or pure carbides [12]. Staining of carbides or carbon-containing nitrides takes place satisfactorily at about 325 K in a few minutes. Pure nitrides are not stained.

Microhardness profiles were determined applying a Leitz Durimet micro-Vickers hardness tester (applied load 100 g). Each hardness value presented is the average of at least ten measurements.

Scanning electron microscopy was performed with a JEOL JXA 50A instrument. After nital etching the specimens were provided with a vapour-deposited gold layer to enhance resolution.

2.6. Microprobe analysis

Applying a JEOL JXA 50A electron microprobe the characteristic N$K\alpha$, C$K\alpha$ and Cr$K\alpha$ intensities were measured. The nitrogen and carbon concentrations were calculated by comparing the N$K\alpha$ and C$K\alpha$ intensities from the specimens to be investigated with those from γ'-Fe_4N and θ-Fe_3C standard specimens respectively, using a linear relation between the weight concentration of the element considered and the corresponding $K\alpha$ intensity. The chromium concentration was calculated by comparing the measured Cr$K\alpha$ intensity with that from a pure chromium standard and applying the standard ZAF correction [13].

2.7. X-ray diffractometry

X-ray diffractometry was performed with a Siemens D500 diffractometer equipped with a graphite monochromator in the diffracted beam and using Cr$K\alpha$ radiation. The residual macrostress was determined according to the $\sin^2\psi$ method [14]. To this end the {2 1 1} line profile of the matrix was recorded according to the preset-time method in steps of 0.03° 2θ employing counting times in the range 40 to 100 sec, depending on the peak intensity. After background elimination and removal of the α_2 component [15] the peak position was determined by fitting a parabola to the intensitives larger than 70% of the maximum intensity (least-squares procedure).

3. Results

The hardened, quenched and tempered, and annealed (initial) structures and the corresponding (nitrided) specimens will subsequently be denoted by "H", "QT" and "A" respectively.

3.1. Morphology

3.1.1. Carbide precipitation

On nitriding, precipitation of particles occurs at grain boundaries (also at martensite–lath boundaries in the H-structure). Dark staining of these particles by Murakami etching (cf. Section 2.5; Fig. 1) and compositional analysis by electron microprobe measurements (6.6 wt % C) suggests, that these particles are carbides of cementite-type structure (cementite contains 6.7 wt % C; for supporting data see [12, 16]). During nitriding this carbide-rich zone moves to larger depths in the specimen (Figs. 2a to c); in the wake of the nitriding front eventually all carbides disappear due to decarburization during nitriding (cf. Section 4.2.1).

At initial stages of nitriding there is a tendency for these carbides to precipitate at grain boundaries parallel to the surface of the specimen (Fig. 3); at later stages this tendency is less pronounced or absent.

3.1.2. Discontinuous and continuous precipitation

In the nitrided zone a discontinuous precipitation reaction proceeds in (small) areas adjacent to the grain boundaries (Fig. 4). The lamellae-like structure within such an area is revealed by scanning electron microscopy (Fig. 5). As a result of ageing globularization of the lamellar nitrides occurs (already apparent in Fig. 5).

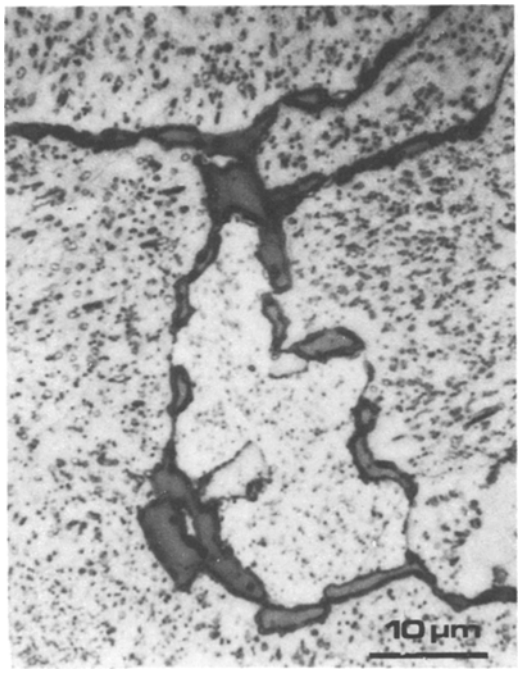

Figure 1 Optical micrograph of a cross section of a nitrided (48 h; 10 vol % NH_3/90 vol % H_2; 803 K) FeCrC (3.16 wt % Cr; 0.20 wt % C) specimen (A-structure; depth below surface 275 µm), showing grain-boundary carbides (stained by Murakami etching).

By analogy with our previous work on nitrided FeCr alloys [10], this structure is thought to be composed of CrN and ferrite; X-ray diffraction analysis performed in the present investigation confirmed the presence of these phases.

As compared to pure FeCr alloys [10], only small areas along grain boundaries are transformed by the discontinuous precipitation reaction in the FeCrC alloy. In the (large) untransformed regions nitride precipitates (whose presence is also deduced from hardness measurements reported in Section 3.2) are apparently of submicroscopical size. The reaction, which took place in these untransformed regions will be denoted by *continuous precipitation* as compared to the *discontinuous precipitation* discussed above (see also [10] for this terminology).

3.1.3. Void and channel formation

On prolonged nitriding, voids develop at grain boundaries in the nitrided zone (Fig. 6). After

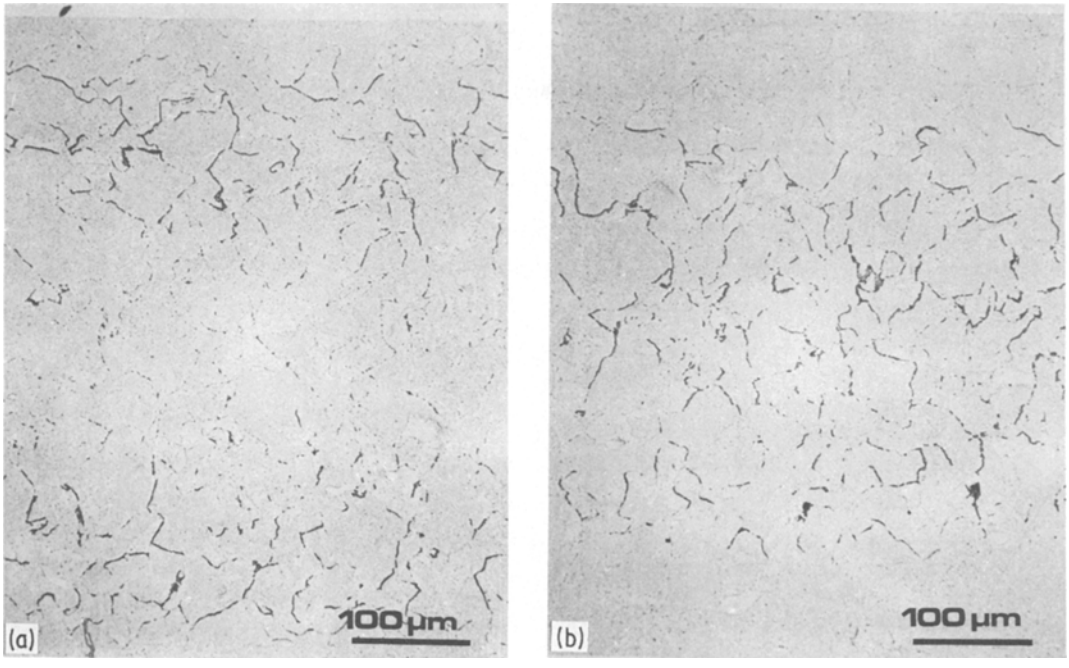

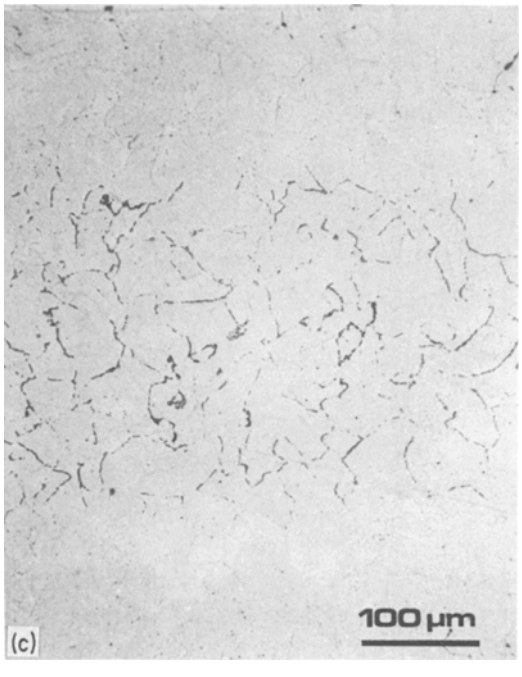

Figure 2 Optical micrographs of the entire cross sections of nitrided (a: 7.5 h, b: 20 h, c: 48 h; 10 vol % NH_3/90 vol % H_2; 803 K) FeCrC (3.16 wt % Cr; 0.20 wt % C) specimens (A-structure). During nitriding carbide-rich zones move to larger depths below the surfaces (carbides stained by Murakami etching).

coalescence of these voids, channel formation along grain boundaries occurs. These channels can be in open contact with the outer atmosphere. Electrodeposition of nickel during specimen preparation for metallographic analysis (Section 2.5) can cause the presence of nickel in channels near the surface (Figs. 7 and 9).

For thin specimens the relative amount of channels is larger than for thick specimens. Furthermore, in thick specimens an orientation perpendicular to the surface is favoured (Fig. 8a), whereas in thin specimens a tendency exists for orientation of the channels parallel to the surface of the specimen (Fig. 8b).

The morphological features discussed in Sections 3.1.1, 3.1.2 and 3.1.3 are deduced from microscopical analyses of the microstructure of the three types of specimens in this investigation (A, QT and H). Because of the initial coarser microstructure of the A-specimens (carbides of about 0.5 μm diameter in a ferritic matrix; see also discussion at start of Section 4) the phenomena are most distinctly observed in cross-sections of nitrided A-specimens.

Finally, an overview of the entire cross-section of a nitrided zone is shown in Fig. 9, demonstrating that the ageing phenomena discussed in Sections 3.1.2 and 3.1.3 are obviously most pronounced in the surface regions, which were nitrided first.

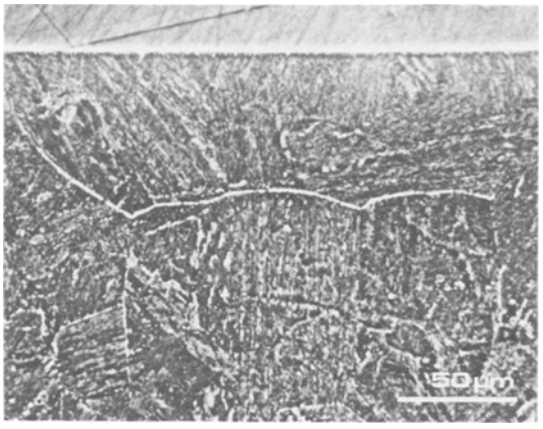

Figure 3 Optical micrograph of a cross section (nital etched) of a nitrided (4 h; 10 vol % NH_3/90 vol % H_2; 803 K) FeCrC (3.16 wt % Cr; 0.20 wt % C) specimen (QT-structure), showing presence of carbides preferentially at grain boundaries more or less parallel to the surface.

3.2. Microhardness profiles

Microhardness–depth profiles of A-, QT- and H-specimens of thickness about 555 μm are shown in Figs. 10a to c for various nitriding times. On nitriding, the surface hardness

Figure 4 Optical micrograph of a cross section (Murakami etched) of a nitrided (210 h; 10 vol % NH_3/90 vol % H_2; 803 K) FeCrC (3.16 wt % Cr; 0.20 wt % C) specimen (A-structure; depth below surface 250 μm), showing regions along grain boundaries transformed by a discontinuous precipitation reaction.

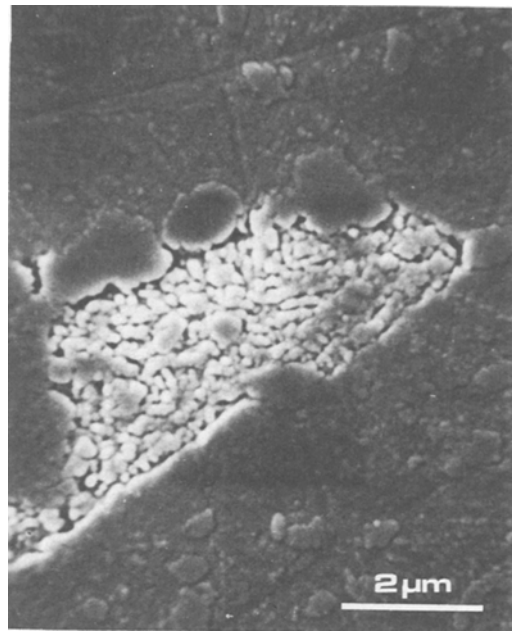

Figure 5 Scanning-electron micrograph of a cross section of a nitrided (48 h; 10 vol % NH_3/90 vol % H_2; 803 K) FeCrC (3.16 wt % Cr; 0.20 wt % C) specimen (A-structure; depth below surface 100 μm), revealing the lamellae-like structure in a region transformed by discontinuous precipitation (cf. Fig. 4).

Figure 6 Scanning-electron micrograph of a cross section of a nitrided (90 h; 10 vol % NH_3/90 vol % H_2; 803 K) FeCrC (3.16 wt % Cr; 0.20 wt % C) specimen (H-structure; depth below surface 40 μm). On prolonged nitriding, voids develop at grain boundaries.

Figure 7 Optical micrograph of a cross section (nital etched) of a nitrided (210 h; 10 vol % NH_3/90 vol % H_2; 803 K) FeCrC (3.16 wt % Cr; 0.20 wt % C) specimen (QT-structure) showing a channel in open contact with the surface. Note electrolytically deposited nickel in that channel (arrow; top of figure coincides with surface).

increases up to a maximum value. For the A-specimens the maximum surface hardness is not reached after the smallest nitriding time (2 h) applied (cf. Fig. 10a with b and c). Continued nitriding (in fact ageing after homogenization) leads to a general reduction of the hardness level. The smallest maximum hardness is observed for the A-specimens.

3.3. Concentration–depth profiles

Coarseness of the microstructure leads to superposition of irregularities on the average concentration profiles. Such irregularities already occur in the initial microstructure of the A-specimens in particular, as revealed by the chromium concentration–depth profile, whereas, within experimental accuracy, a constant chromium concentration is observed for the initial, much finer, QT-structure (Fig. 11; electron microprobe spot size about 2 μm).

The average nitrogen concentration-depth profiles for the A-specimens of thickness about 555 μm are shown in Fig. 12a for various nitriding times. The average nitrogen concentration–depth profiles for the corresponding QT-specimens are shown in Fig. 12b. The data points as measured are also shown in Fig. 12b as an example to indicate the irregularities on the concentration–depth profiles discussed above.

Compared to the QT- (and H-)specimens, the maximum nitrogen surface concentration in the A-specimens is attained more gradually, whereas

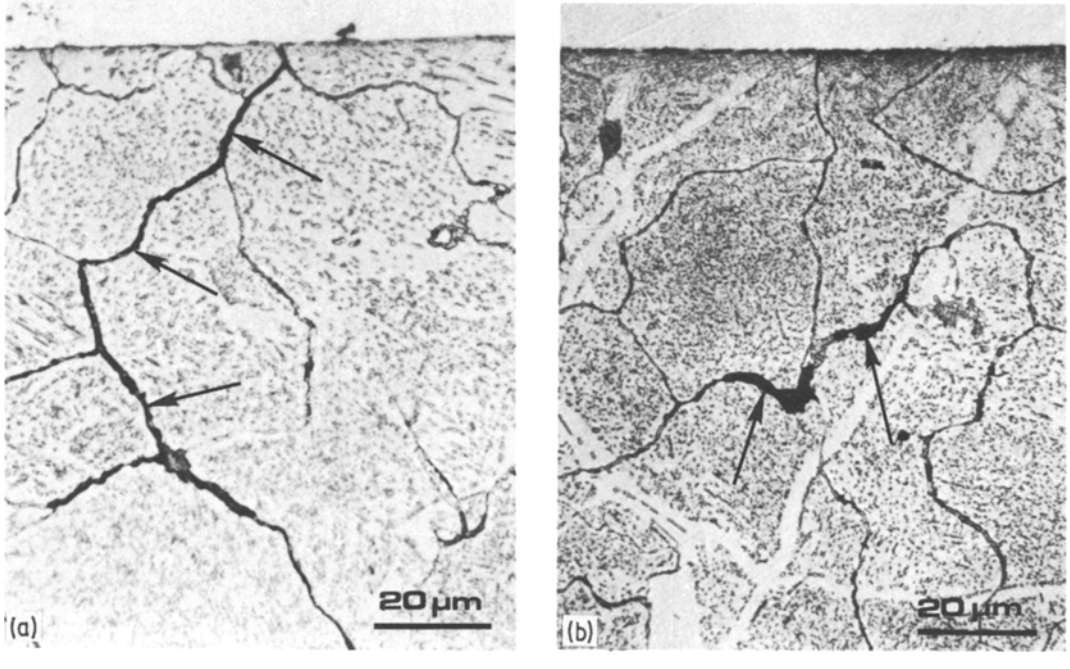

Figure 8 Optical micrographs of cross sections (nital etched) of nitrided (10 vol % NH_3/90 vol % H_2; 803 K) FeCrC (3.16 wt % Cr; 0.20 wt % C) specimens (A-structure). In thick specimens (a, thickness about 550 μm; nitrided for 90 h) channels develop more or less perpendicular to the surface (arrow), whereas in thin specimens (b, thickness about 110 μm; nitrided for 238 h) a tendency exists for orientation of the channels parallel to the surface (arrow).

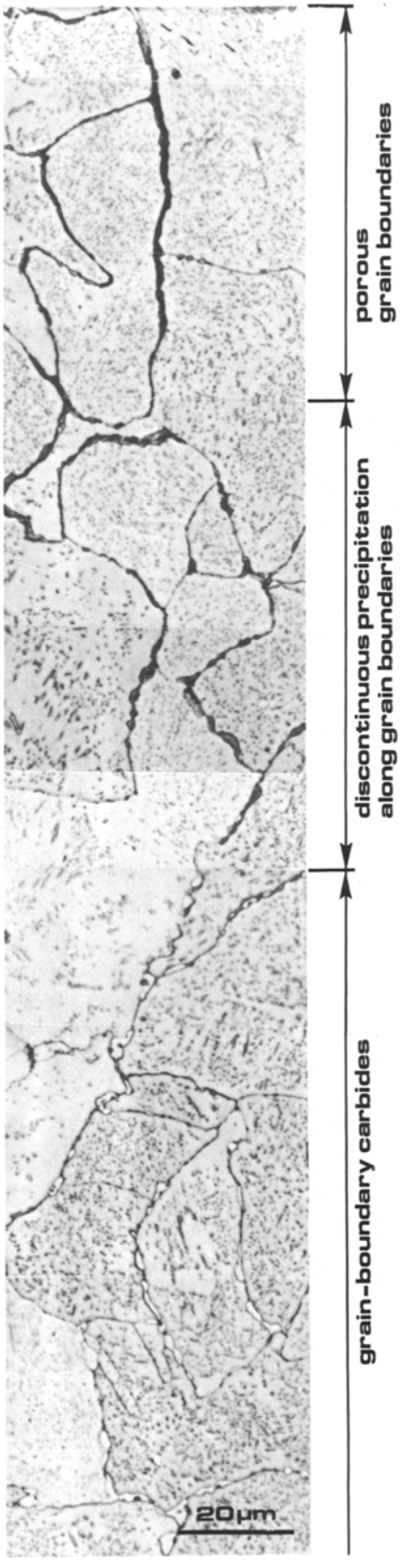

TABLE I Final relative weight gain ($mg\,g^{-1}$) for FeCrC (3.16 wt % Cr; 0.20 wt % C) specimens of various thicknesses. Nitriding conditions: 10 vol % NH_3/90 vol% H_2; 803 K. nd = not determined

Structure	Thickness (μm)			
	110	265	444	555
A	7.9	7.8	7.7	7.65
QT	7.7	7.65	nd	nd
H	7.6	7.6	nd	nd

for a certain nitriding time the largest penetration depth is observed for the A-specimens (cf. Figs. 12a and b).

Carbon concentration–depth profiles of the specimens indicated above are presented in Figs. 13a and b. Large concentration fluctuations are mainly due to grain-boundary carbides (cf. Section 3.1.1) and no attempt has been made to draw average concentration profiles. However, the results confirm the development of coarse carbides, in particular at the nitriding front (cf. Figs. 12 and 13), as well as subsequent decarburization of the nitrided zone (Section 3.1.1).

3.4. Weight gain

The relative weight increases ($\Delta w/w$)* of the A-, QT- and H-specimens are shown as a function of nitriding time in Figs. 14 and 15a and b for the specimens of thicknesses of about 110 and 555 μm, respectively. Obviously the weight of the specimens passes through a maximum on nitriding. This maximum is the larger the thinner the specimen. As compared to the A- and QT-specimens, for relatively small thicknesses the H-specimens show the largest weight maximum (Fig. 14).

In Table I some numerical data are gathered for the final relative weight increase for A-, QT- and H-specimens of various thicknesses.

*All weight changes are given relative to the initial total weight of the specimens. In our previous paper on the nitriding behaviour of FeCr alloys [10] all weight changes were given relative to the weight of the fraction of iron

Figure 9 Optical micrograph of a cross section (nital etched) of a nitrided (48 h; 10 vol % NH_3/90 vol % H_2; 803 K) FeCrC (3.16 wt % Cr; 0.20 wt % C) specimen (A-structure), providing an overview of the microstructural phenomena in the nitrided zone.

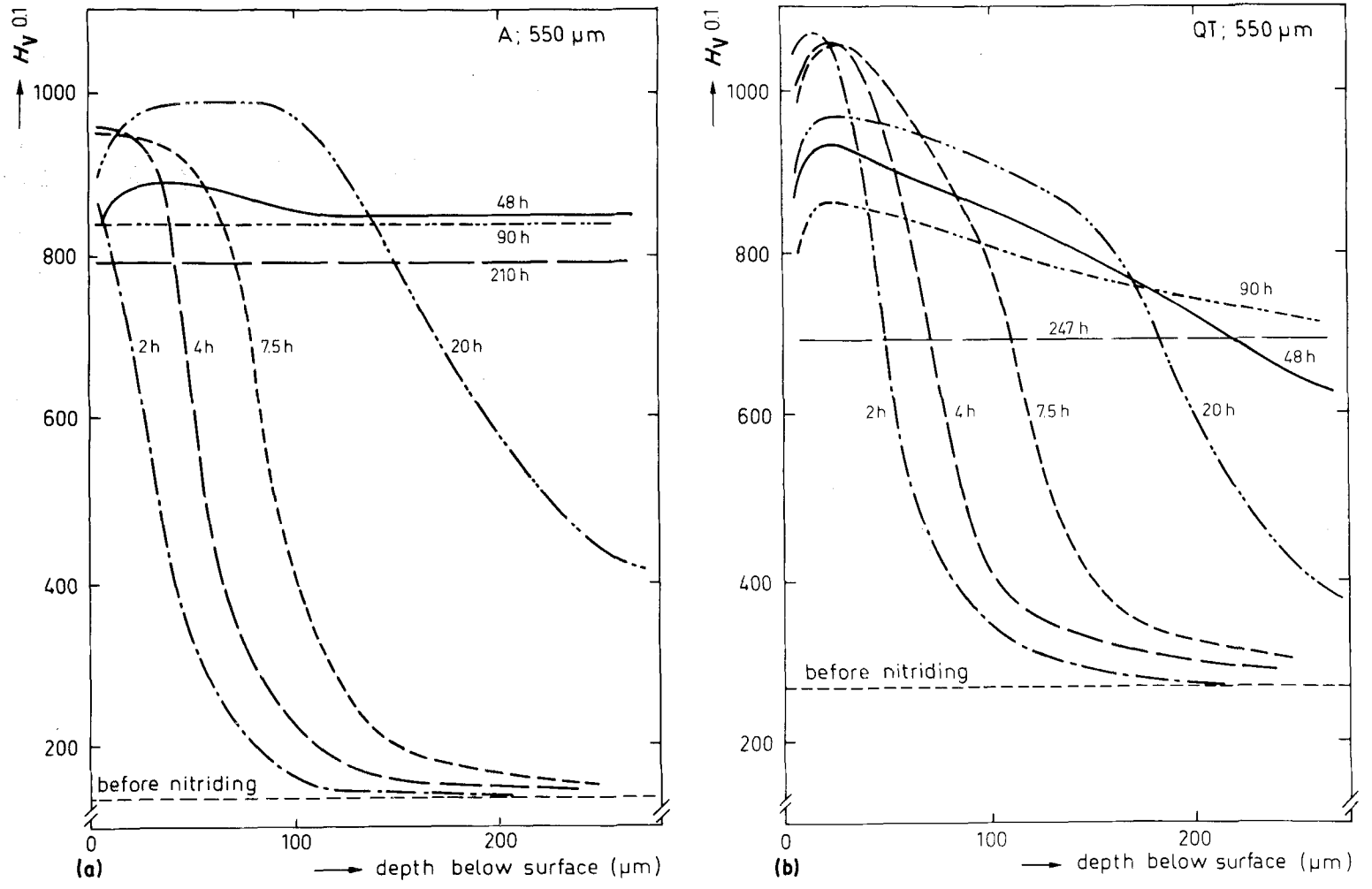

Figure 10 Microhardness profiles of nitrided (10 vol % NH_3/90 vol % H_2; 803 K) FeCrC (3.16 wt % Cr; 0.20 wt % C) specimens (a) A-structure; (b) QT-structure; (c) H-sturcture.

Figure 10 Continued

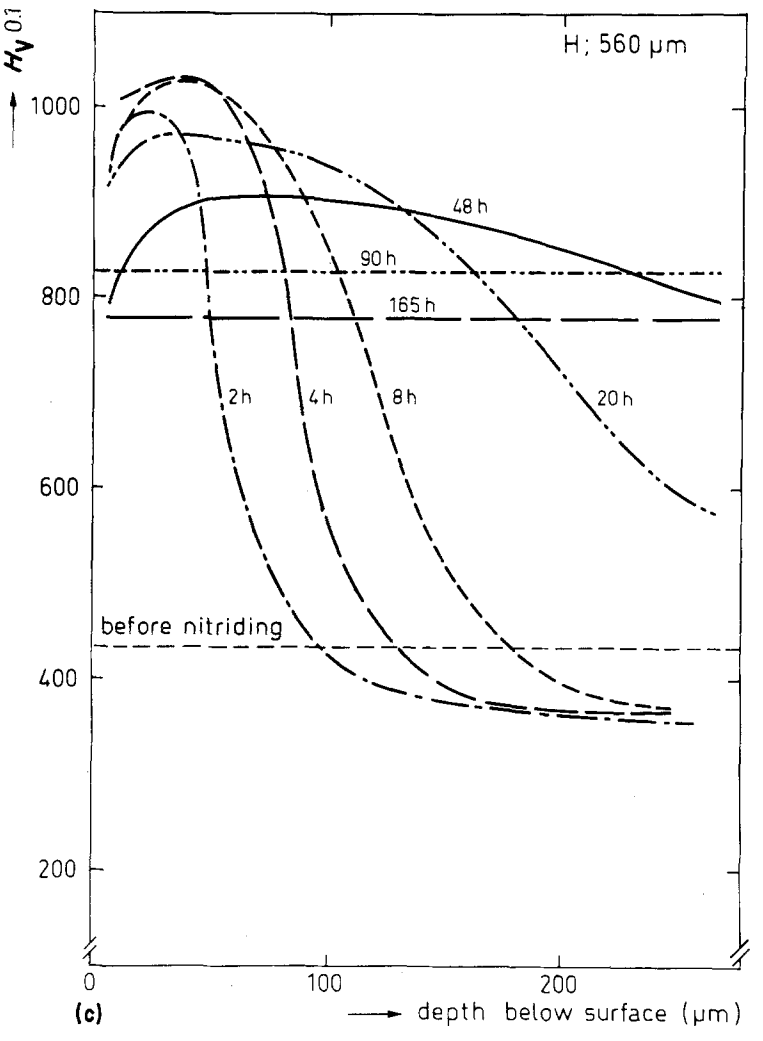

3.5. Thickness increase

The relative thickness increase of the A-specimens is shown as a function of nitriding time in Fig. 16 for various specimen thicknesses. At each curve the time of nitrogen homogenization (as determined from electron microprobe analysis; cf. Fig. 12a) has been marked. In the case of the thinnest specimen (thickness of 108 μm), before homogenization an increase of thickness occurs, whereas after homogenization a thickness decrease is observed at first, which eventually is superseded by a thickness increase. For the thicker specimens a monotonic increase of thickness is observed, which continues after homogenization of the specimens.

In Table II numerical data are gathered for the initial maximum relative thickness increase of the thinnest A-, QT- and H-specimens.

TABLE II Initial maximum relative thickness increase during nitriding (10 vol % NH_3/90 vol % H_2; 803 K) of FeCrC (3.61 wt % Cr; 0.20 wt % C) specimens of thickness about 110 μm (cf. Fig. 16).

Structure	Relative thickness increase (%)
A	2.2
QT	2.0
H	1.8

3.6. Residual surface macrostress

The residual surface macrostress is shown in Fig. 17 as a function of nitriding time for A- and QT-specimens of thickness 3.5 mm. Initially a large compressive macrostress develops in the surface region. On prolonged nitriding this compressive macrostress diminishes and eventually a tensile surface macrostress occurs.

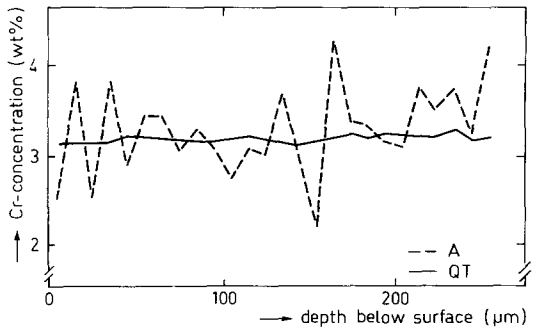

Figure 11 Chromium-concentration profiles (electron microprobe analysis) of FeCrC (3.16 wt % Cr; 0.20 wt % C) specimens of thickness about 550 μm (A- and QT-structure) revealing the initial coarse microstructure of the A-specimens.

4. Discussion

Before the present results on the nitrided FeCrC alloy are discussed, it is convenient to summarize the precipitation sequence occurring on nitriding FeCr alloys as determined in our previous work [10].

1. Initially continuous chromium nitride precipitates of submicroscopical size develop. Owing to long-range strain fields surrounding the coherent precipitates the ferrite matrix is supersaturated with nitrogen: excess-nitrogen.

2. Starting from the grain boundaries, a discontinuous precipitation reaction can occur transforming a ferritic matrix containing coherent chromium nitride particles into a lamellae-like structure of ferrite and incoherent chromium nitride.

3. On prolonged nitriding both the progress of the discontinuous precipitation and the coarsening of the continuous precipitates cause the dissolved excess-nitrogen atoms to segregate at grain boundaries, thereby producing voids containing nitrogen gas.

It should be realized that part of the chromium atoms in the initial A-structure are incorporated in carbides of the type $(Fe, Cr)_7C_3$ as a consequence of the annealing procedure (cf. Section 2.1; [17, 18]). For the present experimental conditions about 2 wt.% chromium will be dissolved in the matrix of the A-specimens, whereas in the H-specimens all chromium (3.16 wt %) will be dissolved [17, 18]. In this connection, the QT-specimens obviously take an intermediate position. Furthermore, during nitriding, tempering of the H-specimens occurs. This implies, that the amount of chromium dissolved in the matrix as experienced at the advancing nitriding front, decreases on nitriding.

4.1. Nitrogen–chromium interaction; nitriding depth and hardness increase

A usual method for characterizing the nitriding depth is to identify it with the hardening depth, $Depth_{HV}$, which can be defined as the depth, where the hardness value equals the average of the maximum (surface region) and the minimum (core region)† hardness. The results thus obtained from Fig. 10 are presented in Fig. 18. (Obviously, in this connection only those nitriding times can be considered, where no overlap of the penetration fronts from both surfaces occurs.) The bold line in Fig. 20 indicates the penetration depth calculated according to the model for *strong* nitrogen–chromium interaction (cf. Equation 1 in [10]). For the A-specimens, especially, $Depth_{HV}$ is smaller than the nitriding depth as predicted by the strong-interaction model.

From the microprobe scans (Fig. 12) the (actual) nitriding depth can be determined. This depth, $Depth_{EMP}$, can be defined as the distance from the surface to the depth where the nitrogen concentration equals half the surface-nitrogen concentration. Corresponding values for $Depth_{HV}$ and $Depth_{EMP}$ are shown in Fig. 19. Clearly for the A-specimens, $Depth_{EMP}$ is appreciably larger than $Depth_{HV}$, whereas for the QT-specimens both measures of nitriding depth yield identical values.

The results shown in Figs. 18 and 19 can be interpreted such that for relatively small amounts of chromium dissolved in the iron matrix (the A-specimens), a *weak* nitrogen–chromium interaction takes place, implying the occurrence of an incubation time for the development of *hardness-increasing* coherent chromium nitride particles. Then the penetration depth of the nitrogen atoms can be much larger than the hardening depth.‡

†In this way the tempering-induced decrease of hardness in the core of the H-specimens is taken into account.

‡This also explains the agreement and disagreement between the measured depth of hardening and the predicted (strong-interaction model) depth of nitriding for the FeCr (3.61 wt % Cr) and the FeCr (1.88 wt % Cr) alloys, respectively, as is apparent from Fig. 12 in [10].

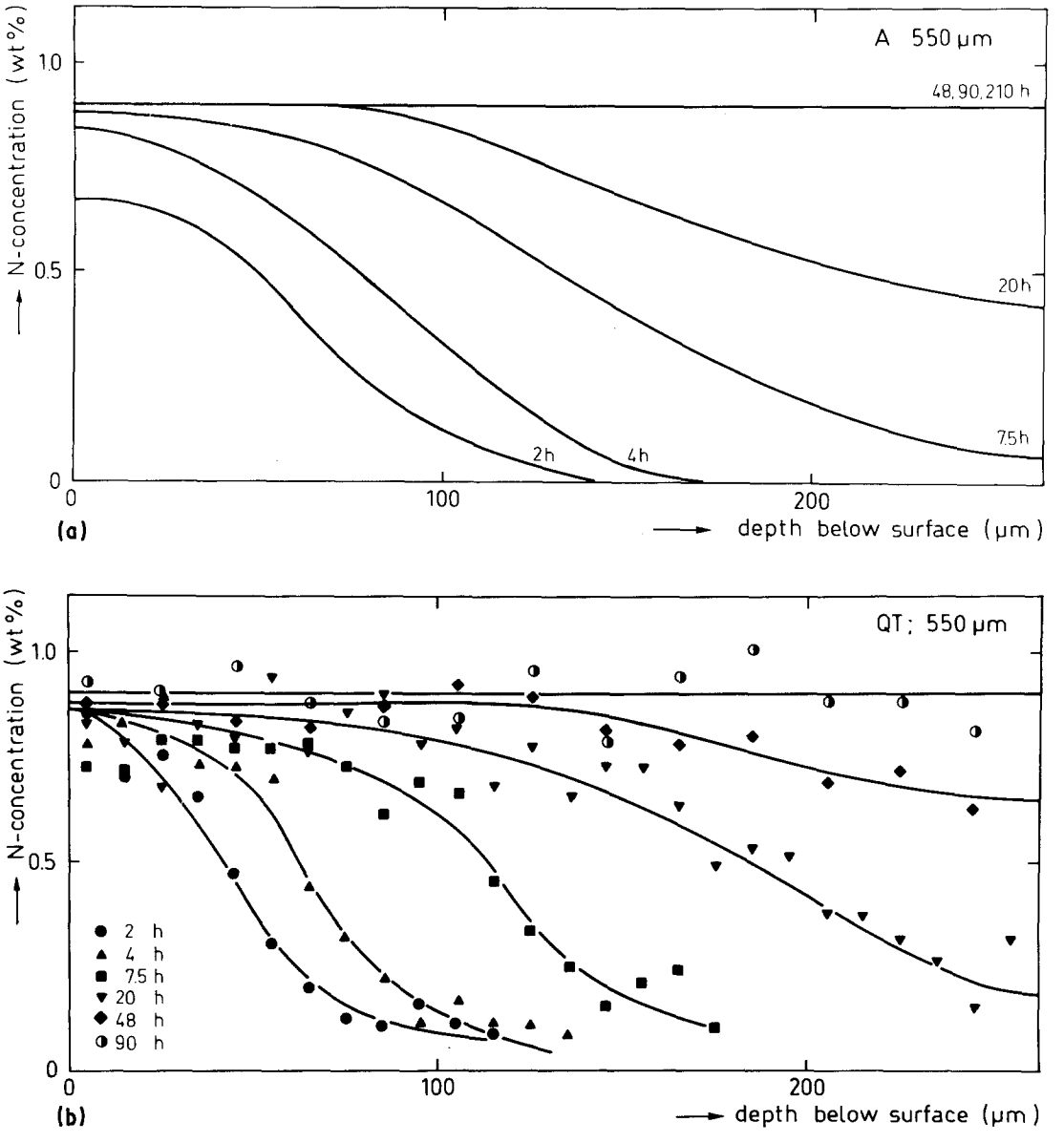

Figure 12 Average nitrogen-concentration profiles (electron-microprobe analysis) of FeCrC (3.16 wt % Cr; 0.20 wt % C) specimens nitrided (10 vol % NH_3/90 vol % H_2; 803 K) for several nitriding times. (a) A-specimens; (b) QT-specimens. For the QT-specimens (b) the data points are also given to indicate the irregularities due to the coarseness of the structure after nitriding.

On nitriding, chromium-containing carbides (in particular in the A-specimens) are transformed into chromium nitride particles. It appears reasonable to assume that this transformation is a slow process as compared to the precipitation of coherent, submicroscopical, chromium nitride particles from chromium atoms dissolved in the ferrite matrix. This assumption is also used elsewhere in the present discussion (Section 4.2.2) and leads to a consistent interpretation of the experimental results. In the A-specimens the smallest amount of dissolved chromium atoms is found. From the above it follows, that, for the same nitriding conditions, the largest nitrogen penetration depth will be observed for the A-specimens (cf. Figs. 12a and b).

Owing to the occurrence of an incubation time for the formation of hardness-increasing coherent chromium-nitride precipitates in the A-specimens, the surface hardness of A-specimens increases gradually on nitriding. Thus

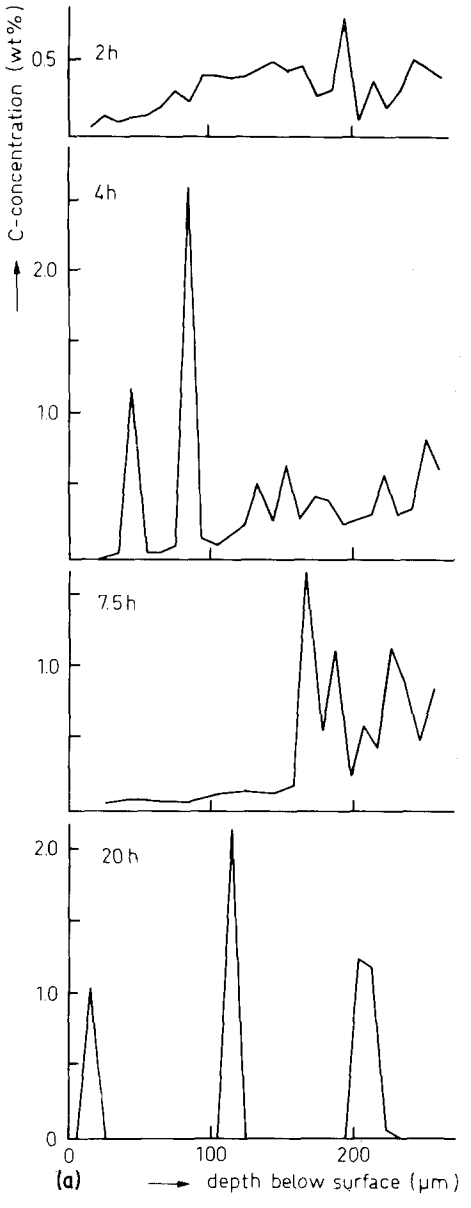

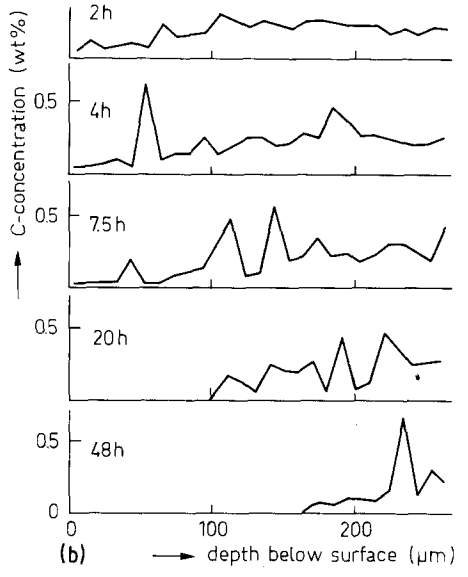

Figure 13 Carbon-concentration profiles (electron-microprobe analysis) of nitrided (10 vol % NH_3/90 vol % H_2; 803 K) FeCrC (3.16 wt % Cr; 0.20 wt % C) specimens of thickness about 550 μm: (a) A-specimens; (b) QT-specimens. The local, very high, carbon concentrations are due to grain-boundary carbides.

the maximum surface hardness of the A-specimens was found at a time (about 20 h), where the surface hardness of the QT- and H-specimens, with respect to their maximal values, had decreased already due to coarsening of the chromium-nitride precipitates (Fig. 10), as has also been found on nitriding binary FeCr alloys [10].

The smallest maximum hardness value is found for the A-specimens (Fig. 10). This can be explained as follows:

1. The smallest amount of coherent chromium-nitride precipitates develop in the A-structure;

and

2. Transformation of (coarse) chromium-containing carbides leads to (coarse) chromium nitrides and (coarse) cementite precipitates (from the carbon atoms released by this chromium nitride formation from chromium-containing carbides; see Section 4.3.2), which do not contribute significantly to an increase of hardness.

4.2. Nitrogen uptake and carbon loss

On nitriding, a rapid increase of weight is observed initially (Figs. 14 and 15). The weight passes through a maximum, decreases slightly and approaches asymptotically a final level. The maximum weight gain by absorption of nitrogen exceeds the expected amount of nitrogen, that can be taken up (denoted by $(\Delta w/w)_{th}$ in Fig. 14), i.e. the amount of nitrogen that forms stoichiometrical CrN, plus the maximum amount of nitrogen that dissolves interstitially in a pure ferritic matrix[§]. The surplus of nitrogen is called *excess-nitrogen* (Section 4.2.3).

The observed decrease of weight on prolonged nitriding is caused by both carbon loss (Section 4.2.1) and partial loss of excess-nitrogen (Section 4.2.3). For the determination of the amount

[§]For thick specimens (e.g. Fig. 15) the maximum weight gain can be smaller than $(\Delta w/w)_{th}$ due to decarburization as dealt with in Section 4.2.1.

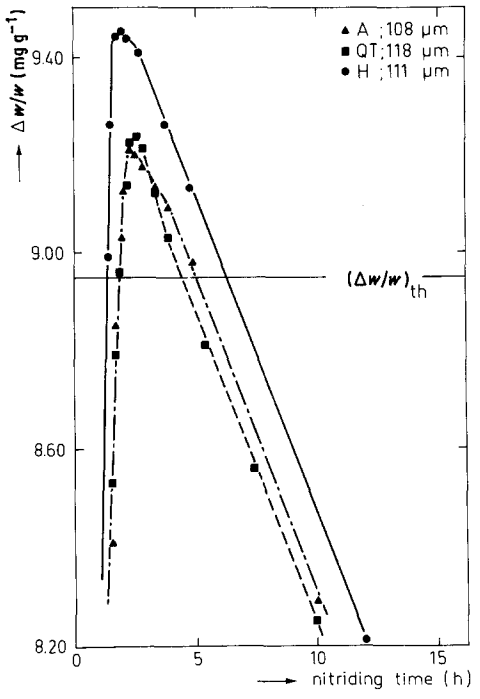

Figure 14 Relative weight increase ($\Delta w/w$) during nitriding (10 vol % NH_3/90 vol % H_2; 803 K) of FeCrC (3.16 wt % Cr; 0.20 wt % C) specimens.

of excess-nitrogen taken up, it is necessary to correct for the decrease of weight gain owing to carbon loss.

4.2.1. Kinetics of carbon loss

Both the electron microprobe analyses (Figs. 13a and b) and the light-microscopical analyses after Murakami etching (e.g. Fig. 2) indicated the occurrence of decarburization during nitriding. The decarburizing rate may be estimated from the decrease of weight of the thin specimens (thicknesses about 110 and 260 μm) after the maximum weight gain is passed, because at these stages these specimens are fully nitrided as follows from a comparison of Figs. 12 and 14¶. Values for the linear decrease of weight after the maximum weight has occurred, are gathered in Table III. This loss of weight is ascribed to decarburization; the loss of excess-nitrogen will be negligible since at these stages no channels in open contact with the outer atmosphere occur (Sections 3.1.3 and 4.2.3). It follows that the decarburization rate is independent of structure (A, QT or H) and thickness of the specimen (average carbon loss: 5.25 $\mu g\,cm^{-2}\,h^{-1}$), implying that a surface reaction (recombination of C and H into, eventually, CH_4 molecules) provides the rate-determining step for decarburization.

Obviously, at final stages of decarburizing, the decarburizing rate will be controlled by the (volume) diffusion of carbon atoms to the surface and no linear decrease of weight as a function of (nitriding) time results.

4.2.2. Kinetics of nitrogen uptake

For the weight increase by nitrogen absorption three kinds of nitrogen can be distinguished in the nitrided zone:

1. Nitrogen in coherent CrN precipitates. The amount of coherent CrN is smallest for the A-structure (smallest amount of chromium initially dissolved in the matrix) and is largest for the H-structure (largest amount of chromium initially dissolved in the matrix);

TABLE III Linear decrease of weight, ascribed to decarburization (Section 4.2.1), after the maximum weight gain has occurred (e.g. Fig. 14). FeCrC (3.16 wt % Cr; 0.20 wt % C) specimens nitrided in a 10 vol % NH_3/90 vol % H_2 gas mixture at 803 K; surface area of specimens = 12 cm^2

Structure	Specimen thickness (μm)	Specimen weight (g)	Time period (h)	Weight loss ($mg\,g^{-1}$)	Rate of carbon loss ($\mu g\,cm^{-2}\,h^{-1}$)
A	108	0.456 941	4 to 10	0.80	5.08
QT	118	0.488 911	3 to 10	0.96	5.58
H	111	0.465 092	3 to 12	1.20	5.17
A	266	1.161 380	12 to 22	0.55	5.33
QT	261	1.072 750	11 to 20	0.54	5.68
H	272	1.206 507	12 to 25	0.92	4.63

¶For estimation of the time for through-nitriding, overlap of two nitrogen-concentration profiles, provoked by nitrogen penetration from both surfaces, should be considered. The time for full nitriding a relatively thin specimen (Fig. 14) is therefore estimated by a (graphical) superposition of two such concentration profiles, each of which can be identified with the concentration profile belonging to one surface as determined for a relatively thick specimen (Fig. 12).

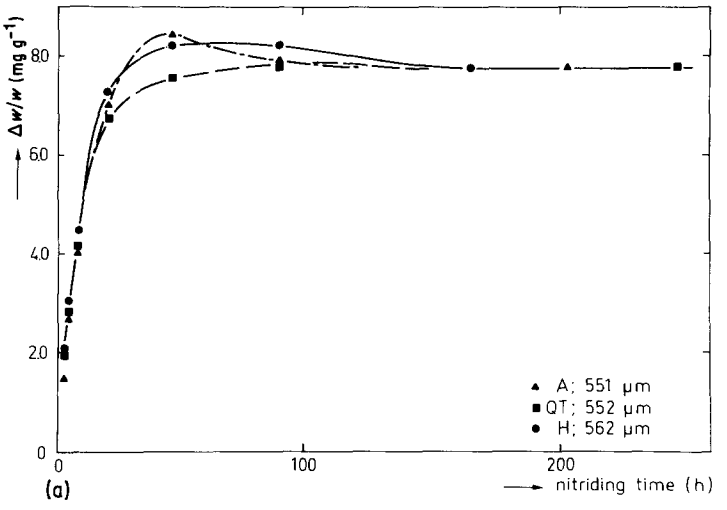

Figure 15 (a) Relative weight increase during nitriding (10 vol % NH_3/90 vol % H_2; 803 K) FeCrC (3.16 wt % Cr; 0.20 wt % C) specimens. (b) Enlargement of (a) for initial period of nitriding.

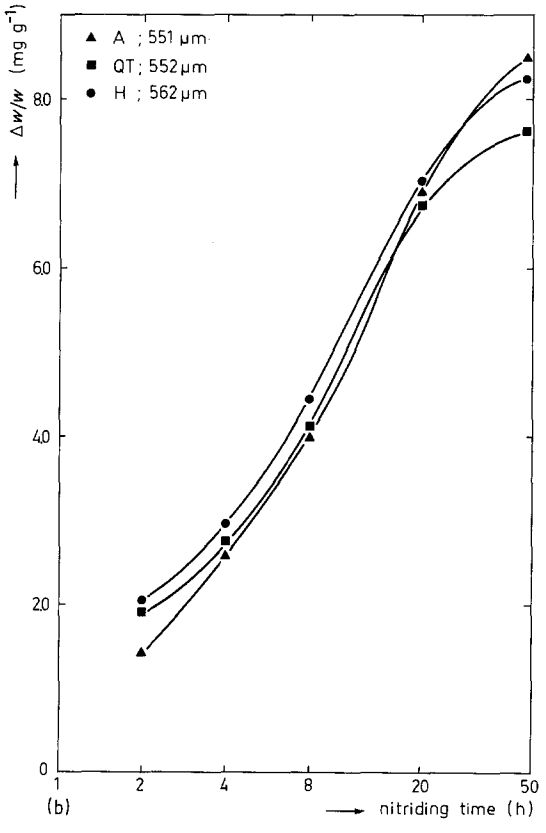

2. Nitrogen in incoherent chromium nitride precipitates resulting from the transformation of chromium-containing carbides. (At later stages of nitriding incoherent chromium nitride particles evolve also by coarsening of coherent chromium nitride particles and by discontinuous precipitation.) The amount of nitrogen in CrN from transformed carbides is largest for the A-structure and smallest for the H-structure; and

3. Nitrogen interstitially dissolved in the ferritic matrix. The amount of interstitially dissolved (excess-)nitrogen is largest for the H-structure and smallest for the A-structure (Section 4.2.3).

The nitrogen-uptake processes corresponding to the nitrogen fractions 1 and 3 are fast as compared to the one corresponding to nitrogen fraction 2 (Section 4.1). It then follows, that the largest initial nitriding rate is found for the H-structure (Fig. 15b).

Obviously, approaching the stage of full nitriding the nitriding rate declines (Fig. 15b). As discussed before, chromium originally dissolved in the matrix is much more rapidly converted into CrN than chromium originally present in carbides. As a consequence, for a certain specimen thickness, H-specimens can be fully nitrided when A-specimens are not (notwithstanding that a fraction of the nitrogen necessary for homogenization reaches the core earlier in the A-specimens than in the H-specimens!; Section 4.1). This implies that at later stages of nitriding the nitriding rate (while continuously decreasing) for the A-structure can be larger than that for the H-structure, as is evident from Fig. 15b. Before the stage of full nitriding is reached, for relatively *thick* specimens, the larger nitriding rate and the larger penetration depth can even lead to a total weight for the A-specimens which is temporarily larger than that of the H-specimens (see Fig. 15): at later stages of nitriding the nitrogen uptake by the A-specimens is governed by the formation of coherent CrN from chromium atoms dissolved in the matrix and the formation of CrN from

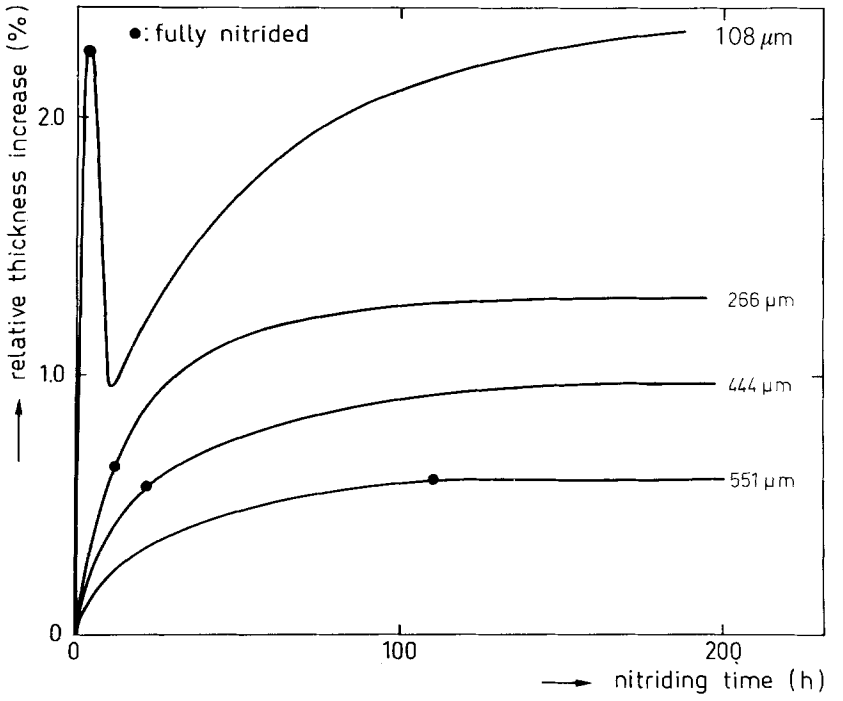

Figure 16 Relative thickness increase during nitriding (10 vol % NH_3/90 vol % H_2; 803 K) FeCrC (3.16 wt % Cr; 0.20 wt % C) specimens of several thicknesses (A-structure). The dot on each curve indicates the moment of full nitriding for the corresponding specimen.

chromium-containing carbides *at and in the wake* of the nitriding front, whereas the nitrogen uptake by the H-specimens is governed by the formation of coherent CrN from chromium atoms dissolved in the matrix *only at* the nitriding front. However, before the stage of full nitriding of relatively *thin* specimens is reached, the nitriding rate for the H-specimens is always largest as a result of the relatively larger contribution of excess-nitrogen to the total weight gain for relatively thin specimens (see next section).

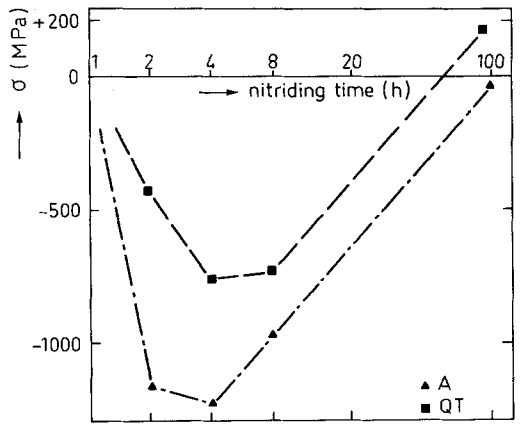

Figure 17 Residual surface macrostresses in nitrided (10 vol % NH_3/90 vol % H_2; 803 K) FeCrC (3.16 wt % Cr; 0.20 wt % C) specimens of thickness about 3.5 mm (A- and QT-structures) as a function of nitriding time.

4.2.3. Excess-nitrogen

In Fig. 20 the maximum weight gain, corrected for carbon loss ($5.25\,\mu g\,cm^{-2}\,h^{-1}$; cf. Section 4.2.1), is given as a function of specimen thickness for the A-, QT- and H-structures. The line, denoted by $(\Delta w/w)_{th}$, indicates the expected amount of nitrogen, that forms stoichiometrical CrN plus the amount of nitrogen, that dissolves interstitially in a ferritic matrix. For all specimens the amount of nitrogen actually taken up exceeds the predicted amount: excess-nitrogen.

Ascribing the existence of excess-nitrogen to the presence of long-range strain fields within the ferritic matrix induced by the misfit between the coherent chromium-nitride precipitates and the matrix [8, 10, 19] and assuming, that all chromium is initially dissolved in the ferritic matrix, a theoretical, maximal, estimate for the amount of excess-nitrogen was calculated using the method (based on thermodynamics of stressed solids) applied to pure FeCr alloys in [10]: $1.03\,mg\,g^{-1}$ (indicated by $(\Delta w/w)^{max}_{excess\text{-}N}$ in Fig. 20). If part of the chromium atoms are

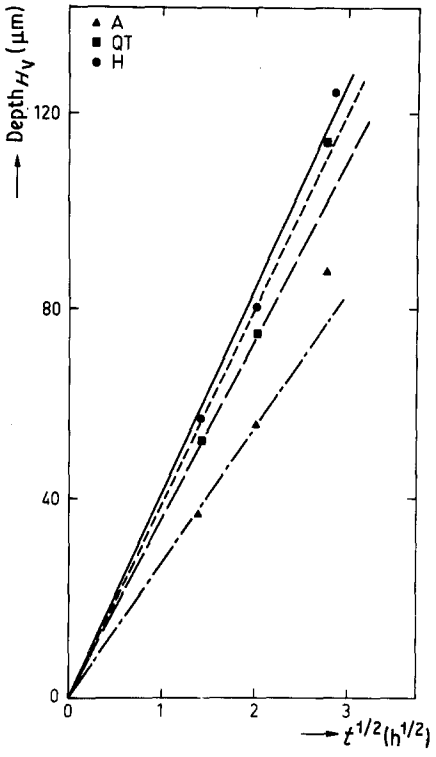

Figure 18 Hardening depth, $Depth_{HV}$ as a function of nitriding (10 vol % NH_3/90 vol % H_2; 803 K) time for FeCrC (3.16 wt % Cr; 0.20 wt % C) specimens of thickness about 555 μm (A-, QT- and H-structure). The bold line indicates the theoretical result for strong nitrogen–chromium interaction, calculated with the following data: diffusion coefficient of nitrogen in ferrite: 5.71×10^{-12} m^2 sec^{-1}; solubility of nitrogen in ferrite: 0.44 mg g^{-1} Fe (cf. [10]).

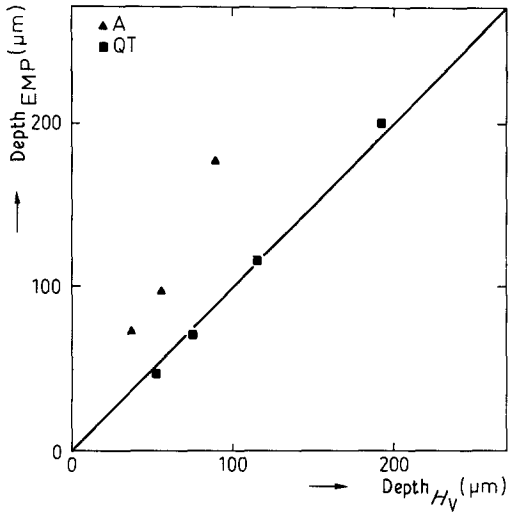

Figure 19 The nitriding depth determined by electron microprobe analysis, $Depth_{EMP}$, versus the hardening depth, $Depth_{HV}$, for nitrided (10 vol % NH_3/90 vol % H_2; 803 K) FeCrC (3.16 wt % Cr; 0.20 wt % C) specimens of thickness about 550 μm.

initially incorporated in carbides, the amount of excess-nitrogen will be smaller. Indeed the amounts of excess-nitrogen are smallest for the A-specimens and largest for the H-specimens (Fig. 20).

On prolonged nitriding the occurrence of discontinuous precipitation* and the coarsening of the continuous precipitates lead to disappearance of the long-range strain fields. Hence a local loss of excess-nitrogen is induced, while the core of the specimen is not yet fully nitrided. These excess-nitrogen atoms can diffuse outward (in the near-surface region) or they diffuse inward to be used for nitriding the core of the specimen. The (relative) amount of former excess-nitrogen atoms used for nitriding deeper layers depends on the specimen thickness: for very thin specimens no significant ageing leading to loss of excess nitrogen has occurred in the surface region at the moment of full nitriding. The amount of excess-nitrogen as determined by weighing is an average over the thickness of the specimen. Hence it follows, that the average amount of excess-nitrogen decreases with increasing specimen thickness (Fig. 20). Extrapolation to zero specimen thickness should lead to the maximum local amount of excess-nitrogen, $(\Delta w/w)^{max}_{excess\text{-}N}$, whereas extrapolation to an infinitely thick specimen should lead to the "theoretical" amount of absorbed nitrogen $(\Delta w/w)_{th}$. It follows from Fig. 20, that the experimentally determined maximal nitrogen uptake indeed obeys the theoretical bounds.

Those former excess-nitrogen atoms, which do not diffuse outward or are not used to nitride the core, segregate at (sub)grain boundaries and coagulate to molecular nitrogen gas, $2(N)_\alpha \rightarrow N_2$, thereby causing voids (the equilibrium pressure of nitrogen gas corresponding to the nitriding gas mixture employed is very high; Fig. 6). Eventually, after coalescence of the voids, channel formation at grain boundaries occurs (Figs. 7 to 9). The utilization of former excess-nitrogen atoms to nitride deeper layers

*The progress of discontinuous precipitation requires *moving* grain boundaries (see Discussion in [10]). As compared to pure FeCr alloys, pinning of grain boundaries in the present FeCrC alloys can easily occur by the existing or developing carbides. This explains the relatively small extent of discontinuous precipitation along grain boundaries in the FeCrC alloys (Section 3.1.2).

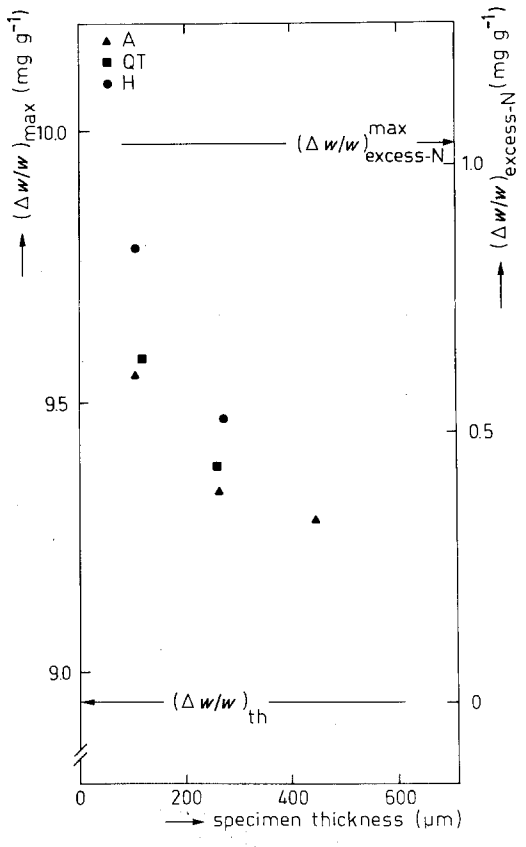

Figure 20 The maximum weight gain corrected for carbon loss (left ordinate) and the amount of excess-nitrogen (right ordinate) for nitrided (10 vol % NH_3/90 vol % H_2; 803 K) FeCrC (3.16 wt % Cr; 0.20 wt % C) specimens as a function of specimen thickness. The line, denoted by $(\Delta w/w)_{th}$, indicates the amount of nitrogen to form stoichiometrical CrN (8.51 mg g^{-1}) + the amount of nitrogen that dissolves interstitially in the ferritic matrix (0.44 mg g^{-1}). The, theoretically calculated, maximum amount of excess-nitrogen (1.03 mg g^{-1}) is indicated by $(\Delta w/w)^{max}_{excess-N}$.

in thick specimens in particular (see above discussion), also explains, that the relative amount of voids/channels is largest for the thinnest specimens (Section 3.1.3 and 4.4).

4.2.4. Final weight gain

As follows from the data gathered in Table I, all final weight gains (determined for the specimens investigated from curves as shown in Fig. 15a) are larger than the theoretical amount, which equals $(\Delta w/w)_{th}$ (Section 4.2.3) minus the total amount of carbon initially present (weight loss by decarburization; Section 4.2.1): 8.95–2.0 = 6.95 mg g^{-1}. In accordance with the previous discussion, for the (over)aged condition considered here, this is ascribed to the presence of former excess-nitrogen in voids. Thus it can also

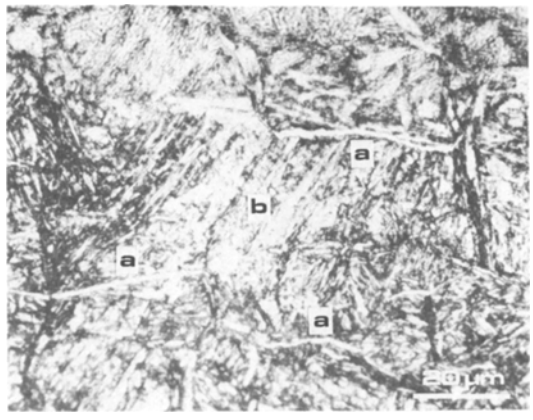

Figure 21 Optical micrograph of a cross section (nital etched) of a nitrided (80 h; ammonia; 783 K) En40B specimen. Carbides are present at grain boundaries more or less parallel to the surface (indicated by "a"). Note absence of carbides at a grain boundary perpendicular to the surface (indicated by "b"). Horizontal direction parallel to the surface.

be understood, that the final weight decreases if the specimen thickness increases, because in a thick specimen a relatively large fraction of the former excess-nitrogen atoms can be used to nitride deeper layers.

This last process will be less substantial for the

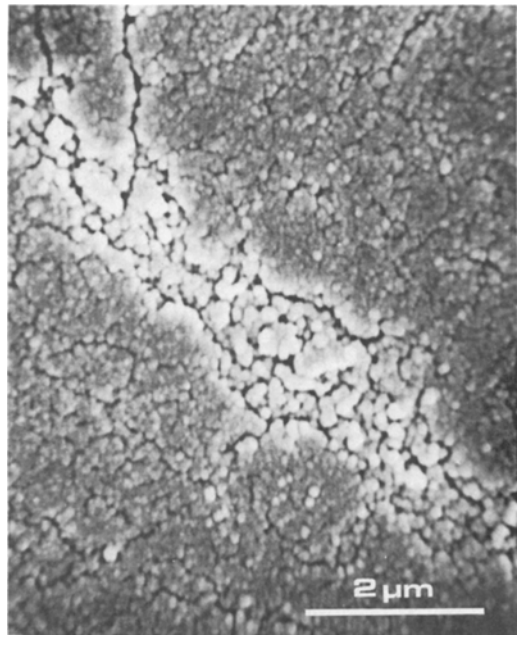

Figure 22 Scanning electron micrograph of a cross section of a nitrided (20 h; ammonia; 783 K) En40B specimen (depth below surface about 150 μm), revealing the lamellae-like structure in a region transformed by discontinuous precipitation (due to ageing globularization of the initially lamellar nitrides occurred; see also Fig. 5).

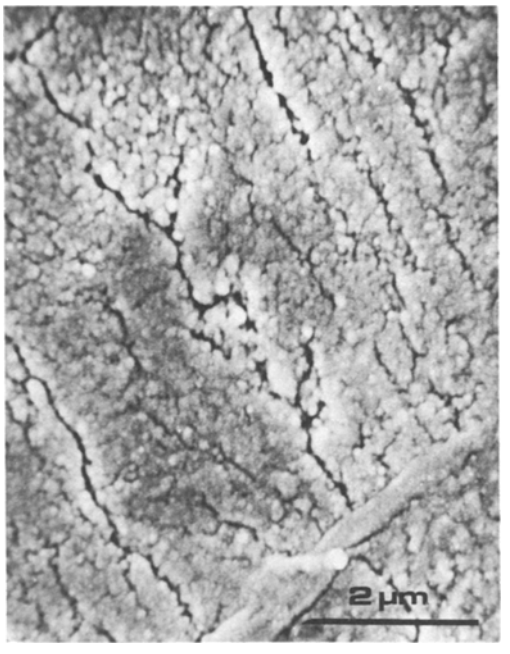

Figure 23 Scanning electron micrograph of a cross section of a nitrided (20 h; ammonia; 783 K) En40B specimen (depth below surface about 35 µm). On prolonged nitriding voids develop at grain boundaries.

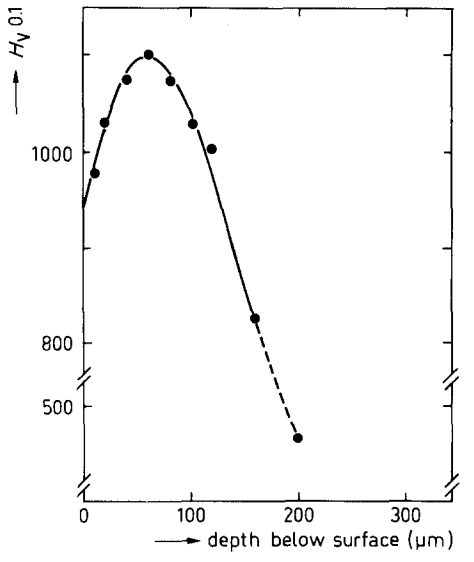

Figure 25 Microhardness as a function of depth below the surface for a nitrided (20 h; ammonia; 783 K) En40B specimen.

A-specimens, since nitrogen penetrates faster in the A-specimens and ageing of the coherent CrN in the A-specimens occurs at a later stage (Section 4.1). On the other hand, the smallest fraction of coherent chromium-nitride particles and hence the smallest maximum *local* amount of excess-nitrogen develops in the A-specimens, since in the A-structure the smallest fraction of initially dissolved chromium atoms occurs (cf. Fig. 20). For the A-specimens considered in Table I the first effect discussed above dominates apparently over the second one: the largest and smallest final weights occur for the A- and H-specimens, respectively.

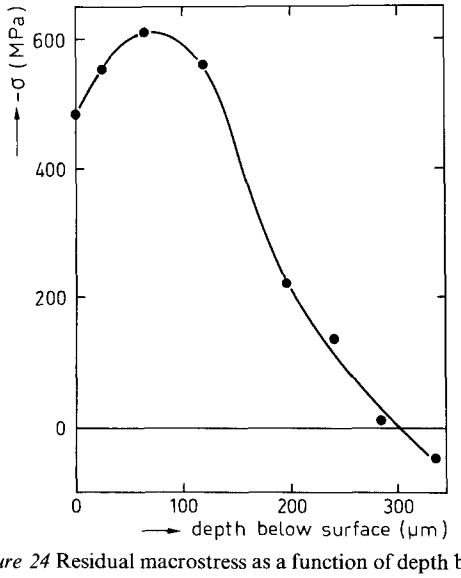

Figure 24 Residual macrostress as a function of depth below the surface for a nitrided (20 h; ammonia; 783 K) En40B specimen.

4.3. Development of residual surface macrostress and consequences thereof

4.3.1. Rise and decline of compressive residual surface macrostress

On nitriding, the nitrided case tends to expand. For an initial structure of FeCrC martensite (H-structure) or FeCr + $(Fe, Cr)_7C_3$ (A-structure) and a final structure of Fe + Fe_3C + CrN volume expansions of about 1.2% (H) and 1.6% (A), respectively, are calculated using crystallographic data given by Pearson [20]. The expansion of the nitrided case is counteracted by the unnitrided core. As a result, normally a compressive residual stress develops near the surface, while a tensile stress evolves in the core [7, 21]†.

The discontinuous precipitation reaction in the nitrided surface layer causes relaxation of

†A compressive residual surface stress is thought to be of beneficial influence on the fatigue resistance, whereas a tensile residual surface stress is considered to have a detrimental effect.

the stresses present at the moment of transformation (cf. recrystallization processes). The corresponding decrease of the compressive residual surface stress will be enhanced by the (continuing) nitriding of deeper layers: the expansion of this latter, (newly) nitrided, zone is counteracted by the (partially) relaxed surface layer and the unnitrided core. On prolonged nitriding the residual surface stress even becomes of tensile nature (Fig. 17)‡.

The ageing, precipitation, process occurs relatively slowly in the A-structure (Section 4.1). Therefore, as compared to the H- and QT-specimens of identical thickness, surface-stress relaxation will take place at a later stage for the A-specimens, and the maximal compressive residual surface stress can be larger for the A-specimens (Fig. 17).

4.3.2. Oriented carbide precipitation

The transformation of chromium-containing carbides at and in the wake of the nitriding front into chromium nitride precipitates releases carbon atoms. This leads to carbide (cementite) precipitation at grain boundaries (Figs. 1 and 2 and Section 3.1.1). The formation of cementite from ferrite and dissolved carbon is accompanied by a volume increase. Then, as a consequence of the initial presence of a compressive macrostress parallel to the surface (Section 4.3.1), cementite precipitation takes place at grain boundaries parallel to the surface (cf. Poisson contraction of matrix; Fig. 3). At later stages of nitriding (corresponding to larger depths) the local compressive residual stress is smaller (due to a larger case/core ratio and the relaxation in the surface region discussed above) and the tendency for oriented precipitation parallel to the surface is less pronounced.

4.3.3. Oriented channel formation

Due to ageing effects (loss of excess-nitrogen) void/channel formation occurs on prolonged nitriding (Figs. 6 to 9 and Sections 3.1.3 and 4.2.3). Obviously void formation implies volume increase. For a relatively thick specimen a tensile surface stress occurs at later stages of nitriding (Section 4.3.1), leading to channel development perpendicular to the surface (Fig. 8a). For a relatively thin specimen the surface stress, although small, can still be of compressive nature at a late stage of nitriding before homogenization (see footnote to Section 4.3.1), implying a small tendency for channel formation parallel to the surface (Fig. 8b).

4.4. Volume changes

Assuming isotropic expansion ($\Delta V/V \simeq 3\Delta l/l$) for the A-specimens a final volume increase of 1.8 to 7% is found (Fig. 16). This dilatation is much larger than that due to the formation of CrN. For the A-structure an expected volume increase of 1.6% was calculated in Section 4.3.1. Even this calculated value is an overestimate, since the slight volume contraction owing to decarburization (cf. Section 4.2.1) has been neglected. Hence, the formation of N_2-filled voids and channels (Section 4.2.3) is thought to be the dominating process for the eventual thickness increase. Because voids develop at later stages of nitriding (Section 4.2.3), a substantial fraction of the dilatation occurs after full nitriding (Fig. 16).

The largest final thickness increase is observed for the thinnest specimens (Fig. 16), because:

1. in thin specimens void/channel formation is more pronounced than in thick specimens (cf. last paragraph of Section 4.2.3); and
2. in thick specimens channel formation perpendicular to the surface is favoured, whereas in thin specimens a tendency exists for channel formation parallel to the surface (Section 4.3.3.).

In a relatively thin specimen the fully nitrided stage can be reached before excessive void/channel formation occurs (Section 4.2.3). Hence, after the occurrence of an (initial) maximum thickness (at the time of full nitriding; Fig. 16) a thickness decrease can occur as a result of decarburization (Section 4.2.1 and Fig. 16) and the loss of some excess-nitrogen through the surface. For the A-, QT- and H-structures the observed maximum thickness increase (about 1.8 to 2.2%; Table II) is about four times the expected maximal increase (0.4 to 0.5%; see Section 4.3.1). On the basis of the above discussion this observation implies the presence of submicroscopical voids in the surface region

‡In thin specimens the occurrence of a *tensile* residual surface stress on prolonged nitriding is unlikely; thin specimens are already fully nitrided before ageing and thus relaxation in the surface region has progressed such far that the constraint imposed by the tendency for expansion in the core could bring about a tensile surface stress.

(where ageing is most pronounced) already at the moment of full nitriding.

5. Conclusions: a model of the nitriding behaviour for iron–chromium–carbon alloys

5.1. General behaviour

1. On nitriding (10 vol % NH_3/90 vol % H_2; 803 K) FeCrC (3.16 wt % Cr; 0.20 wt % C) alloys continuous, hardness-increasing chromium nitride precipitates of submicroscopical size develop from the chromium initially dissolved in the ferritic matrix. Further, transformation of chromium-containing carbides (if present) into incoherent chromium-nitride particles takes place at and in the wake of the nitriding front, thereby releasing carbon atoms, which subsequently precipitate as carbides (cementite) at grain boundaries. In the absence of a compound ("white") layer at the surface, decarburization occurs, eventually leading to the removal of all grain-boundary carbides.

2. Owing to the long-range strain fields surrounding the coherent precipitates, the ferritic matrix is supersaturated with nitrogen: excess-nitrogen. Because the nitrided structure varies with increasing distance from the surface (corresponding to decreasing local nitriding time; see Conclusion 4), the amount of excess-nitrogen depends on depth below the surface. The maximal (local) amount of excess-nitrogen can be estimated applying thermodynamics of stressed solids.

3. Starting from grain boundaries a discontinuous precipitation reaction can proceed, transforming a ferritic matrix containing coherent chromium-nitride particles into a lamellae-like structure of ferrite and incoherent chromium nitride. As compared to pure iron–chromium alloys, the extent of the region which experienced discontinuous precipitation is small as a consequence of less mobile grain boundaries in iron–chromium–carbon alloys owing to pinning.

4. On prolonged nitriding, ageing effects (discontinuous precipitation and coarsening of the continuous precipitates) lead to disappearance of the long-range strain fields and, thus, loss of excess-nitrogen. The former excess-nitrogen atoms either are used for nitriding deeper layers, or segregate at grain boundaries thereby producing voids ($2N_\alpha \rightarrow N_2$) which coalesce to channels, or diffuse outward (near the surface).

5. A compressive residual surface macrostress develops initially by the interaction between the nitrided case, which tends to expand, and the unnitrided core. On prolonged nitriding the discontinuous precipitation reaction contributes to a relaxation of the surface macrostress. Then, continued nitriding of deeper layers can even lead to a surface stress of tensile nature. Consequences of the evolution of macrostress with nitriding time are:

(i) at initial stages of nitriding grain-boundary (cementite) precipitates develop parallel to the surface; on prolonged nitriding this tendency is less pronounced;

(ii) in thick specimens most channels develop perpendicular to the surface, whereas in thin specimens a tendency for channel formation parallel to the surface exists.

5.2. Nitriding response differences between annealed (A), quenched and tempered (QT), and hardened (H) initial structures

6. For a relatively small amount of chromium dissolved in the iron matrix (A-specimens) a *weak* nitrogen-chromium interaction takes place, implying an incubation time for the development of hardness-increasing, coherent, chromium nitride particles. Therefore the nitrogen penetration depth in A-specimens is larger than the hardening depth. For a relatively large amount of chromium dissolved in the iron matrix (QT- and H-specimens) a *strong* nitrogen–chromium interaction takes place.

7. For a certain nitriding time the nitrogen penetration depth is largest for the A-specimens. This is ascribed to the slow transformation of chromium-containing carbides into incoherent chromium nitride particles, as compared to the precipitation of coherent chromium nitride particles from chromium dissolved in the matrix (smallest amount of dissolved chromium occurs in the A-structure).

8. The largest local amount of excess-nitrogen occurs in the H-specimens (the largest amount of initially dissolved chromium atoms occurs in the H-specimens, which leads to the largest amount of coherent chromium-nitride precipitates with accompanying long-range strain fields).

9. The ageing, precipitation process, and the accompanying stress relaxation (Conclusions 4 and 5) occur relatively slowly in the

A-structure (Conclusion 6). Hence, for specimens of the same thickness, the largest compressive residual surface macrostress develops in the A-specimens.

6. Epilogue: Relevance for the nitriding of En40B (also indicated as 24CrMo13)

To illustrate the significance of the present work for the nitriding behaviour of the classical nitriding steel En40B (also indicated by 24CrMo13, containing 0.20 to 0.28 wt % C and 3.00 to 3.50 wt % Cr as major alloying element), in this section the following observations, obtained by nitriding En40B in the quenched and tempered condition, are reported.

1. On nitriding En40B, precipitates develop at grain boundaries in the matrix more or less parallel to the surface (Fig. 21). Previously it was thought that these precipitates consist of γ'-nitride [22, 23] which presence was explained according to the reasoning given below.

The compound layer of En40B is dominantly composed of ε-carbonitride [8, 12]. Beneath the ε-carbonitride compound layer the ferrite matrix then might be supersaturated with respect to γ'-nitride during nitriding. Nucleation of γ'-nitride may occur at energetically favourable places such as former austenite-grain boundaries.

However, the present results clearly demonstrate that these particles are carbides (cementite), which develop from the carbon atoms released by the transformation of chromium-containing carbides into chromium nitrides (Sections 3.1.1 and 4.3.2 and cf. [12, 16]).

With respect to the tendency for alignment *parallel* to the surface of these grain-boundary carbides, as a consequence of (compressive) macrostress development (see Section 4.3.2), note the "empty" grain boundary oriented *perpendicular* to the surface in Fig. 21.

In practice, normally a compound layer develops on the surface of workpieces during nitriding. Such a surface layer is a hindrance to decarburization of the substrate and then the presence of grain-boundary carbides in the nitrided matrix is assured for much later stages of nitriding than in the absence of a compound layer (cf. Fig. 2 and Section 4.2.1).

2. Scanning-electron microscopy revealed the presence of small areas along grain boundaries in a nitrided En40B specimen apparently transformed by a discontinuous precipitation reaction (Fig. 22), as discussed in Sections 3.1.2 and 4.2.3 (due to ageing globularization of the initially lamellar nitrides occurred; see also Fig. 5).

3. The loss of excess-nitrogen on prolonged nitriding, as provoked by coarsening of the chromium nitrides and the occurrence of a discontinuous precipitation reaction, leads to void development along grain boundaries (cf. Section 4.2.3) as is apparent from the nitrided matrix of an En40B specimen (Fig. 23).

4. The behaviour of the residual macrostress as a function of depth below the surface is shown in Fig. 24 for a nitrided En40B specimen. As expected, compressive stresses occur in the surface region whereas, because of mechanical equilibrium requirements, tensile stresses develop in the core [7, 21]. However, as a result of relaxation processes discussed in Section 4.3.1, a decrease of the (compressive) macrostress is observed towards the surface.

5. The behaviour of microhardness as a function of depth below the surface is shown in Fig. 25 for an En40B specimen nitrided analogously to that for Fig. 24. A decrease of hardness is observed towards the surface as was the case with the model experiments (Fig. 10). This can be ascribed to ageing effects (coarsening of chromium nitride particles and the occurrence of discontinuous precipitation; see also [10]).

The surface-adjacent regions showing a decrease towards the surface of both (compressive) macrostress (Fig. 24) and hardness (Fig. 25) coincide. However, it should be recognized that in general there is no direct connection between *macro*stress and hardness, whereas hardness and *micro*stress can be related approximately linearly ([24]; for a more extended discussion see [21]).

Acknowledgements

The authors are indebted to Professor B. M. Korevaar for stimulating discussions and critical reading of the manuscript, and to Messrs P. F. Colijn, P. J. van der Schaaf and D. P. Nelemans for skilful experimental assistance. Dr Ir Th. H. de Keijser and Ing N. M. van der Pers provided X-ray diffraction facilities. Financial support of the Foundation of Fundamental Research of Matter (FOM) is gratefully acknowledged.

References

1. S. A. LEVY, J. F. LIBSCH and J. D. WOOD, "Source book on nitriding" (American Society for Metals, Ohio, 1977).
2. H. C. F. ROZENDAAL, P. F. COLIJN and E. J. MITTEMEIJER, "Proceedings of the conference on Heat Treatment 1984" (The Metals Society, London, 1984) p. 31.1; see also *Surf. Engng.* **1** (1985) 30.
3. T. BELL, *Heat Treat. Met.* **2** (1975) 39.
4. G. WAHL, *Fachberichte Hüttenpraxis Metallweiterverarbeitung* **19** (1981) 1076.
5. E. TAYLOR, *Metall. Prog.* (July) (1983) 1.
6. B. GRELLET, "Proceedings of 3rd International Congress on Heat Treatment of Materials", Shanghai, 1983 (The Metals Society, London, 1984) p. 9.58.
7. E. J. MITTEMEIJER, *J. Heat Treating* **3** (1983) 114.
8. E. J. MITTEMEIJER, H. C. F. ROZENDAAL, P. F. COLIJN, P. J. VAN DER SCHAAF and R. TH. FURNEE, "Proceedings of the Conference on Heat Treatment 1981" (The Metals Society, London, 1983) p. 107.
9. E. J. MITTEMEIJER, A. B. P. VOGELS and P. J. VAN DER SCHAAF, *J. Mater. Sci.* **15** (1980) 3129.
10. P. M. HEKKER, H. C. F. ROZENDAAL and E. J. MITTEMEIJER, *J. Mater. Sci.* **20** (1985) 718.
11. H. DETTNER and J. ELZE, "Handbuch der Galvanotechnik", Vol. 2 (Carl Hanser Verlag, Munich, 1966) p. 102.
12. P. F. COLIJN, E. J. MITTEMEIJER and H. C. F. ROZENDAAL, *Z. Metallkde* **74** (1983) 620 (in English).
13. S. J. B. REED, "Electron Microprobe Analysis" (Cambridge University Press, Cambridge, 1975).
14. H. P. KLUG and L. E. ALEXANDER, "X-ray Diffraction Procedures", 2nd Edn. (Wiley, New York, 1974) p. 755.
15. R. DELHEZ and E. J. MITTEMEIJER, *J. Appl. Crystallogr.* **8** (1975) 609.
16. S. MRIDHA and D. H. JACK, *Met. Sci.* **16** (1982) 398.
17. W. JELLINGHOUSE and H. KELLER, *Archiv. Eisenhüttenw.* **43** (1972) 315.
18. K. KUO, *J. Iron Steel Inst.* **173** (1953) 363.
19. H. H. PODGURSKI and F. N. DAVIS, *Acta Metall.* **29** (1981) 1.
20. W. B. PEARSON, "A Handbook of Lattice Spacing and Structures of Metals and Alloys", Vols. 1 and 2 (Pergamon Press, New York, 1958, 1967).
21. E. J. MITTEMEIJER, Proceedings of the Symposium on "Case-hardened steels: microstructural and stress effects", edited by D. E. Diesburg (TMS-AIME, Warrendale, Pennsylvania, 1984) p. 161.
22. B. J. LIGHTFOOT and D. H. JACK, "Proceedings of the conference on Heat Treatment 1973" (The Metals Society, London, 1975) p. 59.
23. J. ZYSK, J. TOCHIKOWSKI and E. KASPRZYCKA, *Härt.-Techn. Mitt.* **34** (1979) 263.
24. H. C. F. ROZENDAAL and E. J. MITTEMEIJER, in "Eigenspannungen: Entstehung-Messung-Bewertung", edited by E. Macherauch and V. Hauk (Oberursel, Deutsch Gesellschaft für Metallkunde, 1983) p. 363 (in English).

Received 11 January
and accepted 31 January 1985